A GENERAL MULTI-BODY DYNAMIC MODEL TO PREDICT THE BEHAVIOR OF ROLLER CHAIN DRIVES AT MODERATE AND HIGH SPEEDS

MAHN SHIK KIM

Technical Center, Daewoo Motor Company, Inchon, Korea

GLEN E. JOHNSON

Design Laboratory, Mechanical Engineering and Applied Mechanics

University of Michigan, Ann Arbor, MI 48109-2125

encm

UMR1127

A General Multi-Body Dynamic Model To Predict The Behavior Of Roller Chain Drives At Moderate And High Speeds

Mahn Shik Kim

Technical Center, Daewoo Motor Company, Inchon, Korea

Glen E. Johnson

Design Laboratory, Mechanical Engineering and Applied Mechanics,

University of Michigan, Ann Arbor, MI 48109-2125

Abstract

An advanced model in which most important factors of the roller chain drive are considered is developed. Most importantly, for the first time the series of elastic collisions and rebounds that occur as the chain links engage the sprocket is modeled here. Equations of motion are derived in a form very efficient for numerical solution by applying Kane's method. The equations of motion are programmed and used to simulate responses of dynamic roller chain drives.

The dynamic behavior of roller chain drives at moderate and high speeds is studied. Comprehensive observations about the engagement process are presented and discussed. The influence of impact due to collision is investigated. The effects of the center distance and the operation speed on the dynamic behavior of the roller chain are studied, with special attention to the trajectory of the roller chain, the phase between disengagement and engagement, and the transverse vibration.

1 Introduction

Chain drives behave in a very complex manner due to such factors as the discrete nature of the roller chain, non-trivial geometry of the sprocket surface, the impact between the engaging roller and the sprocket, the compliance of the chain, clearances, lubrication, etc.

The motion of roller chain drives at slow speeds has been studied by a kinematic model in which inertia is assumed to be zero and chain span behaves as a rigid bar connecting two polygons made by the sprockets (Morrison, 1952; Bouillon and Tordion, 1965; Chen and Freudenstein, 1988). The motion of this model is often called polygonal motion. The center distance (or, equivalently, the common tangent to the pitch circles of the sprockets) has been identified as an important design variable in this model.

The inertial effects of the roller chain drive become more important as the operating speed increases. Binder and Covert (1948), Ryabov (1968), and Chew (1985) estimated the impact intensity using simplified mathematical models. Turnbull (1974) constructed a test apparatus to measure the angular motion of the sprockets and developed a dynamic model corresponding to his experimental system. Conwell and Johnson (1992) designed a unique machine capable of measuring the bearing force of a sprocket and the strain of the moving chain at the mid-point of a chain link and investigated the effects of preload, transmitted load, and chain speed.

Roller chain drives are subject to periodic excitation from several sources such as polygonal motion, torsional vibration of a sprocket, and unbalance in the drive, etc. These vibrations may be resonant under certain operating conditions. Sack (1954) studied the transverse oscillations in a travelling uniform string pulled over two smooth supports under constant tension and speed. Mahalingam (1957) used the same model as Sack, but also included the centrifugal tension to analyze the resonance of roller chains due to polygonal motion. In another article Mahalingam (1958) investigated the dynamic load in the chain strand due to the polygonal motion, considering the elasticity of the chain and the moment of inertia of the driven system. Choi and Johnson (1992a and 1992b) recently completed the development of an axially moving material model that includes the effects of polygonal action and impact, and is

also capable of incorporating a chain tensioner into the analysis. Some very recent investigations have been reported by Wang (1992) who considered the stability of a chain drive under periodic sprocket excitations, Wang et al (1992) who included inelastic impact in their axially moving material model, and Veikos and Freudenstein (1992) who developed a dynamic model using the Lagrange approach.

Due to the complexity, none of the previous investigations have dealt in a detailed way with the process of the engagement of a chain link with the sprocket. Since the velocity of the roller relative to the seating point on the sprocket is not zero, impact occurs and the roller will rebound on colliding with the sprocket. Then, due to the tension in the chain and the continuing rotation of the sprocket, the roller will approach the sprocket again and collide with the sprocket again, etc. Therefore, the engagement process is not instantaneous; rather, it consists of a series of collisions and rebounds. In the previous investigations, engagement was regarded as instantaneous and collision was regarded as inelastic.

In this paper a refined dynamic model of the roller chain drive is developed in order to study the series of collisions and rebounds of the engaging roller. Other important aspects of dynamic roller chain drives are also considered, including the discrete nature of the chain, geometry of the sprocket and the chain, dynamic engagement and disengagement of chain links, the inertial properties of the roller chain drive, and the friction between the chain links.

The equations of motion are formulated by use of Kane's method so that numerical solutions are obtained in a very efficient way. The resulting equations are programmed and are used to simulate the response of the roller chain drive. Many important characteristics of the roller chain drive at high speeds, such as details of the engagement process, the trajectory of the roller chain, the phase between disengagement and engagement, and transverse vibration, are studied. A parametric study is carried out to investigate the effect of the operational speed and the center distance on the dynamic behavior of the chain span and sprockets. The result obtained here is compared with those obtained by previous investigators.

2 Modeling and Formulation of Equations of Motion

2.1 System Configuration

The model system consists of the drive sprocket, A, the driven sprocket, B, and the tight chain span which transmits power from the drive sprocket to the driven sprocket as shown in Fig. 2.1.

Each sprocket and each chain link is regarded as an independent rigid body. The number of the chain links is N. The value of N is decreased by one as a roller engages with the drive sprocket and is increased by one as a roller disengages from the driven sprocket. Once a link has fully engaged with the drive sprocket, it is disregarded. On the other hand, the link that most recently disengaged from the driven sprocket is regarded as a new rigid body of the system. Since the instants of engagement and disengagement of dynamic chain drives do not necessarily coincide, the number of rigid bodies of the system varies with time. Each rigid body is given an integer for mathematical identification starting with 0 from the drive sprocket. The links next to the drive sprocket and the driven sprocket are rigid bodies 1 and N respectively, and the driven sprocket is rigid body N+1.

The pitch of link i is p^i (i = 1, ..., N), and the radius of the pitch circle of the drive sprocket is p^0 as shown in Fig. 2.1. Similarly, p^{N+1} denotes the radius of the pitch circle of the driven sprocket. Although the pitch of each chain link is assumed to be constant, the superscript is used for convenience in mathematical manipulation. The distance between the mass center of rigid body i and the center of the joint with link i+1 divided by the link pitch is denoted by e^i as shown in Fig. 2.2. Note that $e^0 = 1$ and $e^{N+1} = 0$, whereas $e^i = 1/2$ for i = 1, ..., N. m^i and I^i denote, respectively, the mass and the central moment of inertia of rigid body i. Although the endless roller chain is composed of two different types of links (pin links and roller links) alternately assembled, a single type of link with average inertial properties is assumed in the model.

Modeling of the power supply and power consumption is one of the most difficult aspects of the analysis of dynamic systems. In this analysis no specific type of mechanical element is

considered. Instead, two general types of external inputs are treated. The first type of input is one that makes the speed of the drive sprocket follow a prescribed function. In the second type of input, external torques T_A and T_B are applied to the drive sprocket and the driven sprocket respectively. The energy loss can be attributed to friction at link joints and air resistance. Both viscous friction and Coulomb friction models are used here.

2.2 Equations of Motion

Kane's method is well suited for the formulation of the equations of motion for the model developed here. Note that the number of equations of motion derived by Turnbull (1974) by use of Newton-Euler method is $4(N+2)$, the number of the equations of motion derived by Veikos and Freudenstein (1992) by use of the Lagrange approach is $(2N + 1)$, whereas the number of equations of motion formulated here by use of Kane's method is only $N+2$.

The configuration of the system can be described by a set of generalized coordinates $q_r (r = 0, ..., N+1)$ defined as in Fig. 2.2. The generalized speeds u_r can be chosen as the time derivatives of the generalized coordinates.

$$u_r = \dot{q}_r \tag{2.1}$$

The system is kinematically restrained by the following two constraints.

$$\sum_{j=0}^{N+1} p^j \cos q_j = L\,, \quad \sum_{j=0}^{N+1} p^j \sin q_j = 0 \tag{2.2}$$

Differentiating the constraint equations, Eq. (2.2), with respect to time gives the so-called pseudo-nonholonomic constraints as follows:

$$\sum_{j=0}^{N+1} p^j u_j \sin q_j = 0\,, \quad \sum_{j=0}^{N+1} p^j u_j \cos q_j = 0 \tag{2.3}$$

Thus two generalized speeds u_N and u_{N+1} can be expressed as functions of coordinates q_0, q_1, ..., q_{N+1} and other generalized speeds u_0, ..., u_{N-1} as

$$u_s = \sum_{r=0}^{N-1} A_{sr} u_r + B_s \quad (s = N, \text{ or } N+1) \tag{2.4}$$

where A_{sr} and B_s are functions of the generalized coordinates and the time t defined as

$$A_{sr} = \begin{cases} \dfrac{p^r \sin(q_{N+1} - q_r)}{p^N \sin(q_N - q_{N+1})}, & s = N \\ \dfrac{p^r \sin(q_N - q_r)}{p^{N+1} \sin(q_{N+1} - q_N)}, & s = N+1 \end{cases} \qquad (2.5)$$

$$B_s = 0$$

The angular velocity, $\boldsymbol{\omega}^i$, of rigid body i (i = 0, ..., N+1), and the velocity, $\mathbf{v}^i$, of the mass center of rigid body i can be expressed as

$$\boldsymbol{\omega}^i = u_i \, \mathbf{z} \qquad (2.6)$$

$$\mathbf{v}^i = \sum_{k=0}^{i} \left(1 - \delta_{ki} \, e_i\right) p^k \, u_k \left(-\sin q_k \, \mathbf{x} + \cos q_k \, \mathbf{y}\right) \qquad (2.7)$$

where vectors $\mathbf{x}$, $\mathbf{y}$, and $\mathbf{z}$ are mutually perpendicular unit vectors shown in Fig. 2.1 and δ_{ki} is the Kronecker delta defined according to convention - i.e., 1 for $k = i$ and 0 otherwise.

The angular acceleration, $\boldsymbol{\alpha}^i$, of rigid body i, and the acceleration, $\mathbf{a}^i$, of the mass center of rigid body i are obtained by differentiating Eq. (2.6) and (2.7) with respect to time.

$$\boldsymbol{\alpha}^i = \dot{u}_i \, \mathbf{z} \qquad (2.8)$$

$$\mathbf{a}^i = \sum_{k=0}^{i} \left(1 - \delta_{ki} \, e_i\right) p^k \left(f_x(k) \, \mathbf{x} + f_y(k) \, \mathbf{y}\right) \qquad (2.9)$$

where

$$\begin{aligned} f_x(k) &= -u_k^2 \cos q_k - \dot{u}_k \sin q_k \\ f_y(k) &= -u_k^2 \sin q_k + \dot{u}_k \cos q_k \end{aligned} \qquad (2.10)$$

The partial angular velocities, $\boldsymbol{\omega}_r^i$, and partial velocities, $\mathbf{v}_r^i$, are defined implicitly as

$$\boldsymbol{\omega}^i = \sum_{r=0}^{N+1} \boldsymbol{\omega}_r^i \, u_r + \boldsymbol{\omega}_t^i \qquad (2.11)$$

$$\mathbf{v}^i = \sum_{r=0}^{N+1} \mathbf{v}_r^i \, u_r + \mathbf{v}_t^i \qquad (2.12)$$

By comparing Eq. (2.6) and (2.7) with Eq. (2.11) and (2.12) we have

$$\boldsymbol{\omega}_r^i = \delta_{ri} \, \mathbf{z} \qquad (2.13)$$

$$\mathbf{v}_r^i = \left(1 - \delta_{ri}\, e_i\right) p^r \left(-\sin q_r\, \mathbf{x} + \cos q_r\, \mathbf{y}\right) s(i-r) \tag{2.14}$$

where function $s(\cdot)$ is a unit step function defined as

$$s(j) = \begin{cases} 1, & j \geq 0 \\ 0, \text{ otherwise} \end{cases} \tag{2.15}$$

The r-th generalized holonomic inertia force, F_r^*, of the system is given by

$$F_r^* = \sum_{i=0}^{N+1} \left\{ \boldsymbol{\omega}_r^i \cdot \left(-I^i \boldsymbol{\alpha}^i\right) + \mathbf{v}_r^i \cdot \left(-m^i \mathbf{a}^i\right) \right\} \tag{2.16}$$

It can be shown that Eq. (2.16) can be rearranged using Eq. (2.8), (2.9), (2.13), and (2.14) as

$$F_r^* = \sum_{k=0}^{N+1} h_{rk}\, g(r, k) \tag{2.17}$$

where h_{rk} is a constant defined as

$$h_{rk} = -\delta_{rk} I^r - p^r p^k \sum_{i=r}^{N+1} m^i \left(1 - \delta_{ri} e_i\right)\left(1 - \delta_{ki} e_i\right) s(i-k) \tag{2.18}$$

and $g(r, k)$ is defined as

$$g(r, k) = \dot{u}_k^2 \sin\left(q_r - q_k\right) + \dot{u}_k \cos\left(q_r - q_k\right) \tag{2.19}$$

If we neglect gravity, the r-th generalized holonomic active force F_r of the system can be obtained by

$$F_r = \sum_{i=0}^{N+1} \boldsymbol{\omega}_r^i \cdot T^i\, \mathbf{z} = T^r \tag{2.20}$$

where T^i is the contributing torque exerted on rigid body i. The contributing torque T^i consists of the drive torque, T_A, on sprocket A, the load torque, T_B, on the driven sprocket, and the Coulomb and viscous friction torques on the joints. The viscous friction coefficients of the rotating axles of the drive sprocket and the driven sprocket are d_A and d_B respectively. Friction in the joint occurs between the pin and the bushing. The Coulomb friction coefficient and the viscous friction coefficient of the joint are denoted by μ_{PB} and d_L respectively. Let the x and y components of the force on the rigid body i by rigid body i+1 be X_{i+1} and Y_{i+1} respectively as shown in Fig. 2.2. Then, T^i can be expressed as

$$T^i = \begin{cases} \mu_{PB} R_P \left(X_1^2 + Y_1^2\right)^{1/2} \text{sign}(u_1 - u_0) \\ + d_L(u_1 - u_0) - d_A u_0 + T_A, \text{ for } i = 0 \\ \mu_{PB} R_P \left(X_i^2 + Y_i^2\right)^{1/2} \text{sign}\left(u_{i-1} - u_i\right) \\ + \mu_{PB} R_P \left(X_{i+1}^2 + Y_{i+1}^2\right)^{1/2} \text{sign}\left(u_{i+1} - u_i\right) \\ + d_L \left(u_{i-1} - 2u_i + u_{i+1}\right), \text{ for } i = 1, \ldots, N \\ \mu_{PB} R_P \left(X_N^2 + Y_N^2\right)^{1/2} \text{sign}\left(u_N - u_{N+1}\right) \\ + d_L(u_N - u_{N+1}) - d_B u_{N+1} - T_B, \text{ for } i = N+1 \end{cases} \tag{2.21}$$

where R_P is the radius of the pin.

Values of the joint forces shown in Eq. (2.21) are computed, by the procedure to be explained in Subsection 2.3 below

The r-th nonholonomic generalized inertia force $\tilde{F}_r^*$ (r = 0, ..., $N-1$) and the r-th nonholonomic generalized active force $\tilde{F}_r$ are obtained by the following equations:

$$\tilde{F}_r^* = F_r^* + \sum_{s=N}^{N+1} F_s^* A_{sr} \tag{2.22}$$

$$\tilde{F}_r = F_r + \sum_{s=N}^{N+1} F_s A_{sr} \tag{2.23}$$

Then the Kane's dynamical equations become of the form (Kane and Levinson, 1985)

$$\tilde{F}_r^* + \tilde{F}_r = 0 \tag{2.24}$$

It can be shown that Eq. (2.24) reduces to

$$\begin{aligned} &\sum_{k=0}^{N+1} \left\{ h_{rk} \cos(q_r - q_k) + \sum_{s=N}^{N+1} h_{sk} A_{sr} \cos(q_s - q_k) \right\} \dot{u}_k \\ &= -\sum_{k=0}^{N+1} \left\{ h_{rk} \sin(q_r - q_k) + \sum_{s=N}^{N+1} h_{sk} A_{sr} \sin(q_s - q_k) \right\} u_k^2 \\ &- T^r - \sum_{s=N}^{N+1} T^s A_{sr} \end{aligned} \tag{2.25}$$

Differentiating Eq. (2.3), with respect to time gives

$$\sum_{k=0}^{N+1} p^k \sin q_k \dot{u}_k = -\sum_{k=0}^{N+1} p^k u_k^2 \cos q_k$$
$$\sum_{k=0}^{N+1} p^k \cos q_k \dot{u}_k = \sum_{k=0}^{N+1} p^k u_k^2 \sin q_k \tag{2.26}$$

N equations in Eq. (2.25) and the two equations in Eq. (2.26) constitute non-linear algebraic differential equations of motion of the system. These equations can be solved by a conventional numerical procedure. The derivatives of the generalized speeds, $\dot{u}_k$ (k = 0, ..., N+1), are computed by algebraic solution of the equations of motion. The generalized speeds and the generalized coordinates are then computed by numerical integration. This numerical procedure continues until disengagement of a chain link from the driven sprocket or collision of a roller with the drive sprocket makes the motion of the dynamic model behave differently from the description of the equations of motion formulated above.

Now consider a different case where the drive sprocket is subject to a prescribed motion instead of a prescribed torque. Since $q_0(t)$, $u_0(t)$, and $\dot{u}_0(t)$ are given instead of the torque T_A, Eq. (2.25) and (2.26) can be solved if we neglect the first equation (the equation for $r = 0$) in Eq. (2.25) and regard q_0, u_0, and $\dot{u}_0$ as known variables.

2.3 Computation of Joint Forces

Instantaneous values of the contact forces at the joints can be computed once the instantaneous values of kinematic variables are computed by the numerical procedure explained above.

From the force and moment equilibrium of rigid body i shown in Fig. 2.2, it follows that for i = 0, ..., N+1

$$X_{i+1} - X_i = m^i a_x^i \tag{2.27}$$

$$Y_{i+1} - Y_i = m^i a_y^i \tag{2.28}$$

$$p^i \cos q_i \left\{e^i Y_{i+1} + \left(1-e^i\right) Y_i\right\} - p^i \sin q_i \left\{e^i X_{i+1} + \left(1-e^i\right) X_i\right\}$$
$$= I^i \alpha^i + T^i \tag{2.29}$$

where a_x^i and a_y^i are the **x** and **y** components of the acceleration of rigid body i, and α^i is the magnitude of the angular acceleration. Note that Eq. (2.27) to (2.29) constitute $3(N+2)$ equations, but there are only $2(N+3)$ unknowns and the same number of independent equations. It can be further shown that the six equations for any two consecutive links can be solved independently. Once the six unknown force components in the six equations are solved, the others can be solved sequentially. Tremendous saving in computing time can be made when joint forces are computed in this way.

2.4 Monitoring Engagement and Disengagement

Disengagement of a roller occurs when the contact force between the roller and the sprocket becomes zero. Let C in Fig. 2.3 be the contact point, and **S** be the vector denoting the contact force exerted on the disengaging roller by the sprocket. The location of the contact point C can be determined as shown in the analysis on the contact phenomenon of the roller chain drive by Kim and Johnson (1992). From Fig. 2.3 the force equilibrium in the directions of vectors **x** and **y** can be expressed as

$$\begin{aligned} & S\cos\left(q_{N+1}-\pi-\zeta_B-\psi\right)+X' \\ & =X_{N+1}+m_L R_i u_{N+1}^2\cos\left(q_{N+1}-\lambda_B/2\right) \\ & +m_L R_i \dot{u}_{N+1}\sin\left(q_{N+1}-\lambda_B/2\right) \end{aligned} \tag{2.30}$$

$$\begin{aligned} & S\sin\left(q_{N+1}-\pi-\zeta_B-\psi\right)+Y' \\ & =Y_{N+1}+m_L R_i u_{N+1}^2\sin\left(q_{N+1}-\lambda_B/2\right) \\ & -m_L R_i \dot{u}_{N+1}\cos\left(q_{N+1}-\lambda_B/2\right) \end{aligned} \tag{2.31}$$

where S is the magnitude of contact force vector **S** and X' and Y' are the **x** and **y** components of the joint force on the disengaging link by the neighboring link which is fully engaged with the sprocket. Angles ζ_B, λ_B and ψ are shown in Fig. 2.3

The moment equilibrium about the center of the chain link, point G in Fig. 2.3, can be

expressed as

$$S\{-p_C/2\cos(\lambda_B/2-\zeta_B-\psi)+R_R\sin\psi\}$$

$$-p_C/2\{X'\cos(q_{N+1}-\lambda_B/2)+Y'\sin(q_{N+1}-\lambda_B/2)\}$$

$$=p_C/2\{\cos(q_{N+1}-\lambda_B/2)X_{N+1}+\sin(q_{N+1}-\lambda_B/2)Y_{N+1}\}$$

$$+I_L\dot{u}_{N+1} \tag{2.32}$$

The simultaneous solution of Eq. (2.30) to (2.32) yields values for S, X' and Y'. Disengagement occurs when $S = 0$.

If a link disengages from the driven sprocket, the number of links in the chain span and, therefore, the number of equations in Eq. (2.25) is increased by one. The numerical solution procedure explained in Subsection 2.2 should be interrupted and resumed after the rigid bodies are renumbered, the set of equations of motion are revised accordingly, and the initial conditions for the added chain link are supplied.

Collision is monitored by checking the position of the engaging roller with respect to the surface of the drive sprocket. At the instant of engagement of a roller with the drive sprocket, as shown in Fig. 2.4, one can write

$$q_1-q_0+\lambda_A/2+\pi/2=0 \tag{2.33}$$

The left side of Eq. (2.33) will be called the separation angle. The separation angle is always greater than or equal to zero (Eq. 2.33 holds at the instant of engagement) and it will be refered to again in the discussion of the engagement process in Section 4 below.

If the relative speed of a collision falls within a prescribed limit, the collision can be regarded as the final collision and forthcoming collisions are neglected in the computation. In this case the engaging link is given the same angular velocity as the sprocket and rebound is not allowed by setting the coefficient of restitution to zero. Then, the roller engaged becomes a part of the drive sprocket, and the engagement process of a roller is completed. At this moment the number of rigid bodies of the system is decreased by one. The numerical solution procedure in Subsection 2.2 is restarted after the rigid bodies are renumbered.

2.5 Computation of Separation Velocity of the Colliding Roller

The velocities of the rigid bodies at the final moment of collision are computed from equations governing the collision process. In this analysis, the equations governing collision are derived by the approach based on the coefficient of restitution (Wehage and Haug, 1982; Brach, 1981). If collision occurs, the numerical solution procedure explained in Subsection 2.2 should be restarted at the instant of rebound with new values of generalized speeds.

Let C and C', in Fig. 2.4, be the points that come into contact with each other at the instant of collision. Then, the velocity $\mathbf{v}^C$ of point C on the sprocket can be expressed as

$$\mathbf{v}^C = \mathbf{v}_0^C u_0 \tag{2.34}$$

where

$$\mathbf{v}_0^C = p_0 \{-\sin(q_0 - \lambda_A)\,\mathbf{x} + \cos(q_0 - \lambda_A)\,\mathbf{y}\} + R_R \{\sin(q_0 - \lambda_A + \zeta_A)\,\mathbf{x} - \cos(q_0 - \lambda_A + \zeta_A)\,\mathbf{y}\} \tag{2.35}$$

The velocity $\mathbf{v}^{C'}$ of point C' is expressed as

$$\mathbf{v}^{C'} = \mathbf{v}_0^{C'} u_0 + \mathbf{v}_1^{C'} u_1 \tag{2.36}$$

where

$$\mathbf{v}_0^{C'} = p_0 (-\sin q_0\,\mathbf{x} + \cos q_0\,\mathbf{y}) \tag{2.37}$$

$$\mathbf{v}_1^{C'} = p_1 (-\sin q_1\,\mathbf{x} + \cos q_1\,\mathbf{y}) + R_R \{\sin(q_1 + \nu)\,\mathbf{x} - \cos(q_1 + \nu)\,\mathbf{y}\} \tag{2.38}$$

where ν is the angle between link 1 and normal vector $\boldsymbol{\rho}$ and equal to $\zeta_A + \pi/2 - \lambda_A/2$.

Let t_1 be the instant at which points C and C' come into contact with each other. We can define the velocity of approach, $\mathbf{v}_{app}$, of points C and C' at time t_1 as

$$\mathbf{v}_{app} = \mathbf{v}^{C'}(t_1) - \mathbf{v}^C(t_1) \tag{2.39}$$

Since the velocity of approach is not zero, impact occurs between the roller and the sprocket.

Let t_2 be the final moment of the collision process. From Eq. (2.24) we have

$$\int_{t_1}^{t_2} \tilde{F}_r^*\, dt = \int_{t_1}^{t_2} \tilde{F}_r\, dt \qquad (r = 0, \ldots, N-1) \tag{2.40}$$

Assuming that $t_1 \approx t_2$ we have, from Eq. (2.16) and (2.22) and several other equations derived in Subsection 2.2,

$$\int_{t_1}^{t_2} \tilde{F}_r^* \, dt$$

$$= \sum_{k=0}^{N+1} \left\{ h_{rk} \cos(q_r - q_k) + \sum_{s=N}^{N+1} h_{sk} A_{sr} \cos(q_s - q_k) \right\} \{ u_k(t_2) - u_k(t_1) \} \tag{2.41}$$

Neglecting forces and torques that remain constant during the time interval from t_1 to t_2, we have

$$\int_{t_1}^{t_2} \tilde{F}_r \, dt = \int_{t_1}^{t_2} \tilde{\mathbf{v}}_r^C \cdot \mathbf{R}^C \, dt + \int_{t_1}^{t_2} \tilde{\mathbf{v}}_r^{C'} \cdot \mathbf{R}^{C'} \, dt \tag{2.42}$$

where $\tilde{\mathbf{v}}_r^C$ and $\tilde{\mathbf{v}}_r^{C'}$ are r-th nonholonomic partial velocities of points C and C' respectively, and $\mathbf{R}^C$ and $\mathbf{R}^{C'}$ are contact forces exerted on points C and C' respectively. Since $t_1 \approx t_2$, $\tilde{\mathbf{v}}_r^C$ and $\tilde{\mathbf{v}}_r^{C'}$ are nearly fixed in the inertial reference frame and nearly equal to their values at time t_1. And since $\mathbf{R}^C = -\mathbf{R}^{C'}$, we have

$$\int_{t_1}^{t_2} \tilde{F}_r \, dt = \left(\tilde{\mathbf{v}}_r^{C'} - \tilde{\mathbf{v}}_r^C \right) \cdot \int_{t_1}^{t_2} \mathbf{R}^{C'} \, dt \tag{2.43}$$

where

$$\tilde{\mathbf{v}}_r^C = \begin{cases} \mathbf{v}_0^C, \, r = 0 \\ 0, \, r = 1, \ldots, N-1 \end{cases}, \quad \tilde{\mathbf{v}}_r^{C'} = \begin{cases} \mathbf{v}_0^C, \, r = 0 \\ \mathbf{v}_1^C, \, r = 1 \\ 0, \, r = 2, \ldots, N-1 \end{cases} \tag{2.44}$$

From Eq. (2.40), (2.41) and (2.42) we obtain the following N equation for $r = 0, \ldots, N-1$.

$$\sum_{k=0}^{N+1} \left\{ h_{rk} \cos(q_r - q_k) + \sum_{s=N}^{N+1} h_{sk} A_{sr} \cos(q_s - q_k) \right\} u_k(t_2)$$

$$- \left(\tilde{\mathbf{v}}_r^{C'} - \tilde{\mathbf{v}}_r^C \right) \cdot \boldsymbol{\rho} I_\rho - \left(\tilde{\mathbf{v}}_r^{C'} - \tilde{\mathbf{v}}_r^C \right) \cdot \boldsymbol{\tau} I_\tau$$

$$= \sum_{k=0}^{N+1} \left\{ h_{rk} \cos(q_r - q_k) + \sum_{s=N}^{N+1} h_{sk} A_{sr} \cos(q_s - q_k) \right\} u_k(t_1) \tag{2.45}$$

where I_ρ and I_τ are the magnitudes of the normal impulse and the tangential impulse

respectively, or

$$I_{\rho} = \boldsymbol{\rho} \cdot \int_{t_1}^{t_2} \mathbf{R}^{C'}\, dt\,, \quad I_{\tau} = \boldsymbol{\tau} \cdot \int_{t_1}^{t_2} \mathbf{R}^{C'}\, dt \tag{2.46}$$

The two scalar constraint equations in Eq. (2.3) should be satisfied at time t_2. Thus we have

$$\sum_{j=0}^{N+1} p^j \sin q_j\, u_j(t_2) = 0\,, \quad \sum_{j=0}^{N+1} p^j \cos q_j\, u_j(t_2) = 0 \tag{2.47}$$

The velocity of separation $\mathbf{v}_{sep}$ of points C and C' at time t_2 can be defined as

$$\mathbf{v}_{sep} = \mathbf{v}^{C'}(t_2) - \mathbf{v}^{C}(t_2) \tag{2.48}$$

Two assumptions that experiments have shown are valid in many situations of practical interest are now introduced. First, it is assumed that the normal components of $\mathbf{v}_{app}$ and $\mathbf{v}_{sep}$ have opposite directions and the magnitude of the normal component of $\mathbf{v}_{sep}$ is proportional to that of the normal component of $\mathbf{v}_{sep}$. In other words,

$$\boldsymbol{\rho} \cdot \mathbf{v}_{sep} = -\, e\, \boldsymbol{\rho} \cdot \mathbf{v}_{app} \tag{2.49}$$

Or,

$$\begin{aligned} &\boldsymbol{\rho} \cdot \left(\mathbf{v}_0^{C'} - \mathbf{v}_0^{C}\right) u_0(t_2) + \boldsymbol{\rho} \cdot \mathbf{v}_1^{C'} u_1(t_2) \\ &= -e \left\{ \boldsymbol{\rho} \cdot \left(\mathbf{v}_0^{C'} - \mathbf{v}_0^{C}\right) u_0(t_1) + \boldsymbol{\rho} \cdot \mathbf{v}_1^{C'} u_1(t_1) \right\} \end{aligned} \tag{2.50}$$

where e, the coefficient of restitution, is the constant of proportionality. The coefficient of restitution is assumed to depend on material properties, but velocity dependence is ignored.

Second, it is assumed that slipping occurs between the roller and the sprocket at time t_2 and the tangential impulse is proportional to the normal impulse.

$$I_{\tau} = -\, \mu_{RS}\, I_{\rho} \tag{2.51}$$

where μ_{RS} is the coefficient of kinetic friction between the roller and the sprocket.

The generalized speeds at the instant of rebound, $u_k(t_2)$ (k = 0, ..., N+1), and the magnitudes of the normal impulse and the tangential impulse, I_{ρ} and I_{τ} respectively, can be obtained by solving N+4 algebraic equations represented by Eq. (2.45), (2.47), (2.50), and

(2.51) simultaneously.

3 Simulation of the Responses of Chain Drives

The equations formulated in Section 2 are programmed and used to simulate the response of the roller chain drive for a range of conditions. No. 40 chain and No. 80 chain parameters are used in the simulation. Each chain is used with two identical sprockets to compose a roller chain drive system. Center distance varies from 19.5 to 20.5 pitches in the No. 40 chain systems and 13.5 to 14.5 pitches in the No. 80 chain systems with the increment of 0.1 pitch respectively.

Two different types of driving mechanism are used in the simulation. Constant torques are used in the first type. In the second type, torques are given by two torsion bars connecting the sprockets with two gears rotating at constant speeds. The second type represents the so-called four square drive mechanism of the physical system used by Turnbull (1974). The angles of rotation, $q_A(t)$ and $q_B(t)$, of the gears connected to the drive sprocket and the driven sprocket respectively are linear functions of the time, t. Then, the external torques can be expressed as

$$T_A = k\left(q_A(t) - q_o\right), \quad T_B = k\left(q_B(t) - q_{N+1}\right) \tag{3.1}$$

where k is the torsional stiffness of the torsion bars.

Two different variations of friction are used for each chain as shown in Table 3.1. Two different values of viscous friction are assumed for the No. 40 chain system. It turned out that most characteristics observed in the system with large viscous friction were also retained in the system with smaller friction. The difference caused by the type of friction was also tested with No. 80 chain systems as in Table 3.1. The test showed very little difference in the responses of the system between the friction models (as long as the friction remains small).

The parameters shown in Table 3.1 are used in the text and in the figures from here on, unless otherwise stated. The configuration of the system with No. 80 chain with torsion bar drive mechanism and Coulomb friction is the same as that of the experimental system used by Turnbull (1974). The value of coefficient of restitution is selected as 0.75 which is within a typical range for steel to steel collision(Goldsmith, 1960). Some of the parameters in Table 3.1

are used to describe the properties of the chain drives simulated and the others are used to set precision and accuracy of computation.

The computational burden required for the proposed simulation was so immense that careful arrangement in many aspects of the numerical procedure was necessary. More detail in this regard can be found in the dissertation of the first author of this paper (Kim, 1990).

4 Results

In this section, results of the analysis are presented and compared to those reported in previous works. The speed shown in the text and the figures in this section denotes the steady state angular speed of the drive sprocket unless otherwise stated.

4.1 Engagement Process

Fig. 4.1 shows the angular speed of the engaging chain link (link 1), the angular speed of the drive sprocket, and the separation angle[1] between the engaging chain link and the drive sprocket for a No. 80 chain system with viscous friction at approximately 384 rpm. It is shown that the engagement of a roller with the drive sprocket involves a series of collisions and rebounds.

As is mentioned earlier, the engagement process has been modeled by a single inelastic collision in previous work. Response of an inelastic collision model is different from that of an elastic collision model as shown in Fig. 4.2. A No. 80 chain system with Coulomb friction and common tangent of 13.5 pitches is simulated at approximately 750 rpm. Coordinate x used in Fig. 4.2 directs from the center of the drive sprocket to that of the driven sprocket. The centers of the drive sprocket and the driven sprocket are located at $x = 0$ and $x = .24765$ m respectively. The chain link moves from the right to the left in the figure.

It can be observed that the inelastic collision model not only neglects all collisions except the first one but also underestimates the impulse of the first collision. In this particular example, the impulse on the drive sprocket due to inelastic collision is approximately half that due to the

[1]The separation angle is defined as the left hand side of Eq. (2.33).

first elastic collision. Interestingly, Turnbull (1974) reported that the experimental values of the angular acceleration and the changes in angular speeds of the sprockets were two to three times larger than the values computed from his dynamic model of inelastic collision.

Fig. 4.3 shows the step changes in the angular velocities of chain links due to collisions in the first engagement process shown in Fig. 4.2. Only the first six collisions are shown in Fig. 4.3. Disengagement occurred between the second collision and the third collision in this particular case. It can be observed that the influence of impact on the change in angular velocity is limited to the first two links and the last two links in the chain span. The second chain link from each end experiences an angular speed change almost equal but opposite to that experienced by the first link from the same end. The two links next to the drive sprocket experience much larger velocity changes than those next to the driven sprocket.

The results presented above are quite different from those predicted by the simplified collision models posed by Ryabov (1968) or Chew (1985). They predicted that the magnitude of the change in angular velocity decreases progressively with the distance from the engaging roller.

4.2 Trajectory of the Roller Center

Fig. 4.4 shows a typical trajectory of the center of a roller of a No. 40 chain system with larger friction at various speeds as well as that of the kinematic model (massless polygons connected by a rigid coupling bar) for the common tangents of 19.5 and 20 pitches. The trajectory is presented in a rectilinear coordinate system, (x, y). The center of the drive sprocket is (0, 0) whereas that of the driven sprocket is (.24765 m, 0) for the common tangent of 19.5 pitches and is (.254 m, 0) for the common tangent of 20.0 pitches.

It can be observed that, in general, the trajectory of the roller center deviates more from that of the kinematic model as speed increases. The most significant deviation can be found near the driven sprocket. Because of its inertia the chain link does not follow the path predicted by the kinematic theory immediately after it disengages from the driven sprocket. Instead, it further rotates in the same direction as the driven sprocket (the direction it has rotated before it

disengages) before it reverses its rotation to approach the drive sprocket. When Conwell (1989) studied the moving chain with a Kodak Ektapro High Speed Motion Analyzer, this detouring action of the chain roller was observed as a kink.

As the speed increases the trajectory becomes smooth in the middle of the span because of increased inertial effects. The trajectory near the drive sprocket is also different from that of the kinematic model. At the instant of the first collision of the engaging roller, the chain link attains larger angular position and larger angular speed in the direction of rotation of the drive sprocket than predicted by the kinematic theory. This phenomenon contributes to the delay of engagement and the decrease in the colliding speed between the sprocket and the roller.

The trajectories at 100 rpm in Fig. 4.4 show amplified transverse motion of the chain span, especially at the common tangent of 20.0 pitches. This is due to the transverse vibration of the chain and will be discussed further in Subsection 4.4. The trajectory becomes less affected by the center distance as speed further increases.

4.3 Phase Between Disengagement and Engagement

As mentioned earlier, previous investigations indicated that the length of the common tangent (or, equivalently, the center distance between two sprockets) strongly influences the performance of chain drives (Turnbull, 1974; Chen and Freudenstein, 1988; Mahalingam, 1958). In the kinematic model engagement and disengagement are completely in phase if the common tangent is an integral number of pitches whereas they are completely out of phase if the common tangent is an odd number of half pitches.

But, the simulation result indicates that the phase between disengagement and engagement of the dynamic chain drives is dependent not only on the length of common tangent but also on the operation speed as in Fig. 4.5(b). The phase defined here as shown in Fig. 4.5(a) is a measure that quantifies how early disengagement occurs compared to the first collision of each engagement process.

The phase change due to the operation speed can be readily explained. The chain span deviates more from the straight line as the speed increases. As the speed increases, the angle of

the drive sprocket at which engagement occurs gets larger while the angle of the driven sprocket at which disengagement occurs gets smaller. Thus the distance between the end points of the chain span increases as the speed increases. Due to these facts the length of the chain span measured along the chain span is always longer than the length of the chain span of the kinematic model. Accordingly, the difference (and therefore the phase) between disengagement and engagement grows larger as the speed increases (see Fig. 4.5(b)). At high speeds it is even possible for there to be several more chain links in the chain span than would be predicted by the kinematic model.

4.4 Transverse Vibration of the Chain Span

To investigate the transverse vibration of the dynamic model, the speed of the simulated system is steadily increased from a speed far less than the theoretical fundamental natural frequency to a speed exceeding three times the fundamental natural frequency.

First, a No. 40 chain system with larger friction and common tangent between 19.5 and 20.5 is simulated. The fundamental natural frequencies computed by the formula derived by Mahalingam (1957) are 84.7 and 82.6 rpm for the common tangent of 19.5 and 20.0 pitches respectively. Engagement and disengagement are most in phase for 19.9 pitches and most out of phase for 20.4 pitches in this particular system due to the change in the phase between disengagement and engagement as is explained in Subsection 4.3.

The y coordinates of the instantaneously lowest and highest points in the chain span gave a useful description of the vibration. Fig. 4.6 shows time-varying y coordinates of the two extreme points for selected common tangent and range of speeds. The transverse motion near the fundamental frequency is maximized and minimized for the common tangent of 19.9 pitches and 20.4 pitches respectively instead of 20.0 pitches and 20.5 (or 19.5) pitches respectively as the kinematic model predicts.

No further amplification of the transverse motion was observed up to approximately 320 rpm at any center distance.

Similar results are obtained for the No. 80 chain system except that amplification is

maximized and minimized when the common tangent is 14.0 and 13.5 pitches respectively. Note that for these values of common tangent disengagement and engagement are most in phase and most out of phase respectively, since the phase change of this particular system remains small.

This result agrees with the observation of Turnbull (1974). He reported that resonance occurred, in both simulation and experiment, only when the tooth frequency is the same as the fundamental frequency and the common tangent is an integral number of pitch.

However, it should be noticed that the phase between disengagement and engagement is better suited than the common tangent for predicting the resonance of the roller chain at moderate and high speeds. If the change in phase between disengagement and engagement is significant, the prediction of resonance by the kinematic theory will be unreliable. The analysis presented here is the first one with adequate detail to make the computation of the change in phase between the engagement and disengagement possible.

Fig. 4.7 shows the trajectory of a roller center, the chain tension, and the deviation of the chain span from a straight line for the No. 40 chain with a common tangent of 19.9 pitches (for which the largest amplification was observed). The dashed lines in the chain tension plot denote the discontinuities by impact during the engagement process. The fluctuation in the chain tension and the deviation of the chain span from a straight line contain a strong harmonic component of twice the frequency of engagement cycle. This is in accordance with the theories based on the moving band subject to a periodic chain tension. They predict that more vigorous resonance occurs when the frequency of excitation is twice the natural frequency of the transverse motion of the chain than when the former is the same as the latter (Mahalingam, 1957; Naguleswaran and Williams, 1968).

It can be observed that transverse vibration of the No. 40 chain system with a common tangent of 19.9 pitches or 20 pitches is amplified a little bit, as shown in Fig. 4.6, at around 45 rpm which is approximately half the natural frequency. Note that this amplification below the natural frequency is not explained by linear vibration theory. In nonlinear systems resonance

below the natural frequency is possible and called subharmonic vibration (Stoker, 1950).

5 Conclusions

The advanced dynamic model developed here has provided a useful tool to investigate the behavior of roller chain drive at moderate and high speeds. Use of Kane's method to formulate the equations of motion has made the numerical solution procedure very efficient. Facets of the behavior of the dynamic roller chain drive have been unveiled by the analysis presented here.

It has been confirmed that engagement of the chain link consists of a series of collisions and rebounds. Details of the engagement process and more reasonable assessment of the influence of the impact due to the series of collisions involved in the engagement process have become available.

A detailed picture of the motion of the chain links in the chain span has also been obtained. The effect of the operation speed on the changes in the trajectory of the chain link and in the timing of disengagement and engagement have been presented.

Transverse vibration of the chain span appears to be more significantly affected by design parameters than any other performance measures at moderate and high speeds. Transverse vibration of the chain span is more directly affected by the phase between disengagement and engagement than by the length of common tangent. The more the operation speed increases, the more the phase between disengagement and engagement deviates from the value computed by the kinematic model. The comprehensive model presented here is a viable tool for computation of the change in the phase between disengagement and engagement.

6 Acknowledgement

The authors gratefully acknowledge the support of the National Science Foundation through grants no. MSM-88-12957 and MSM-89-96293.

References

Binder, R. C. and Covert, W. V., 1948, "Impact between Chain Roller and Sprocket in a Chain Drive," *Journal of Franklin Institute*, Vol. 245, No. 4 , pp 319-329.

Bouillon, G. and Tordion, G. V., 1965, "On polygonal Action in Roller Chain Drives," ASME *Journal of Engineering for Industry*, Vol. 87B, pp. 243-250.

Brach, R. M., 1981, "Moments Between Impacting Rigid Bodies," ASME *Journal of Mechanical Design*, Vol. 103, pp. 812-817.

Chen, C. K. and Freudenstein, F., 1988, "Towards a More Exact Kinematics of Roller Chain Drives," ASME *Journal of Mechanisms, Transmission, and Automation in Design*, Vol. 110, No. 3, pp. 123-130.

Chew, M., 1985, "Inertial Effects of a Roller-Chain on Impact Intensity," ASME *Journal of Mechanisms, Transmission, and Automation in Design*, Vol. 107, pp. 123-130.

Choi, W. and Johnson, G. E., 1992a, *Vibration of Roller Chain Drives at Low, Medium and High Operating Speeds*, MEAM Technical Report Number XXXXXXX, University of Michigan, Ann Arbor, Michigan.

Choi, W. and Johnson, G. E., 1992b, *Transverse Vibrations of a Roller Chain Drive with Tensioner*, MEAM Technical Report Number XXXXXXX, University of Michigan, Ann Arbor, Michigan.

Conwell, J. and Johnson, G. E., 1992, *Experimental Investigation of Chain Tension and Roller Sprocket Impact Forces in Roller Chain Drives*, MEAM Technical Report Number XXXXXXX, University of Michigan, Ann Arbor, Michigan.

Conwell, J., 1989, *An Examination of Transient Forces in Roller Chain Drives*, Ph. D. dissertation, Vanderbilt University, Nashville, Tennessee.

Gear, C. W., 1971, *Numerical Initial Value Problems in Ordinary Differential Equations*, Prentice-Hall, Englewood Cliffs, New Jersey.

Goldsmith, W., 1960, *Impact*, Edward Arnold Ltd., London.

Harding, L. J., 1979, "Numerical Analysis and Application Software Abstracts," *Computing Center Memo* 407, The University of Michigan Computing Center.

Hindmarsh, A. C., 1975, *GEAR: Ordinary Differential Equation System Solver*, Lawrence Livermore Laboratory, UCID-30001, Rev. 3.

Kane, T. R. and Levinson, D. A., 1985, *Dynamics: Theory and Applications*, McGraw-Hill.

Kim, M. S., 1990, Dynamic Behavior of Roller Chain Drives at Moderate and High Speeds,

Ph. D. dissertation, University of Michigan.

Kim, M. S. and Johnson, G. E., 1992, "Mechanics of Roller Chain - Sprocket Contact: Parts 1 and 2," *Proceedings of the 1992 International Power Transmission and Gearing Conference, DE-Vol. 43-2*, ASME, NY, pp 689 -702.

Mahalingam, S., 1957, "Transverse Vibrations of Power Transmission Chains," *British Journal of Applied Physics*, Vol. 8, pp. 145-148.

Mahalingam, S., 1958, "Polygonal Action in Chain Drives," *Journal of Franklin Institute*, Vol. 265, No. 1, pp. 23-28.

Morrison, R. A., 1952, "Polygonal action in Roller Chain Drives," *Machine Design*, Vol. 24, No. 9, pp. 155-159.

Naguleswaran, S. and Williams, C. T. H., 1968, "Lateral Vibrations of Bandsaw Blades, Pulley Belts, and the Like," *International Journal of Mechanical Science*, Vol. 10, pp. 239-250.

Ryabov, G. K., 1968, "Inertial Effects of Impact Loading in Chain Drives," *Russian Engineering Journal*, Vol. 48, No. 8, pp. 17-19.

Sack, R. A., 1954, "Transverse Oscillations in Travelling Strings," *British Journal of Applied Physics*, Vol. 5, pp. 224-226.

Stoker, J. J., 1950, *Nonlinear Vibrations in Mechanical and Electrical Systems*, Interscience Publishers, New York.

Turnbull, S. R., 1974, *The Dynamic behavior of Roller Chain Drive*, Ph. D. Dissertation, University of Newcastle upon Tyne, U. K.

Veikos, N. M., and Freudenstein, F., 1992, On the Dynamic Analysis of Roller Chain Drives: Parts 1 and 2," *Mechanism Design and Synthesis, DE-Vol. 46*, edited by G. Kinzel et al, ASME, NY, pp 431 - 450.

Wang, K. W., 1992, "On the Stability of Chain Drive Systems Under Periodic Sprocket Oscillations," *ASME Journal of Vibration and Acoustics*, Vol. 114, pp 119 - 126.

Wang, K. W., et al, 1992, "On the Impact Intensity of Vibrating Axially Moving Roller Chains," *ASME Journal of Vibration and Acoustics*, Vol. 114, pp 397 - 403.

Wehage, R. A. and Haug, E. J., 1982, "Dynamical Analysis of Mechanical System with Intermittent

Motion," ASME *Journal of Mechanical Design*, Vol. 104, pp. 778-784.

Specification	No. 40 chain		No. 80 chain	
	Larger friction	Smaller friction	Viscous friction	Coulomb friction
Number of teeth on the sprocket	24		25	
Mass of the chain link	8.34×10^{-3} kg		6.9×10^{-2} kg	
Chain pitch	1.27×10^{-2} m		2.54×10^{-2} m	
Radius of the roller	3.97×10^{-3} m		7.94×10^{-3} m	
Radius of the pin	1.99×10^{-3} m		3.97×10^{-3} m	
Central mass moment of inertia of the sprocket	4.97×10^{-4} kg-m^2		0.238 kg-m^2	
Central mass moment of inertia of the chain link	3.89×10^{-7} kg-m^2		1.13×10^{-5} kg-m^2	
Loaded torque on the driven sprocket	9 N-m		340 N-m	
Friction coefficient between the roller and the sprocket	0.1		0.1	
Coefficient of restitution for the roller and the sprocket	0.75		0.75	
Torsional stiffness of the torsion bar	N/A	N/A	N/A	1460 Nm/rad
Damping coefficient of link joint	0.01	0.001	0.001	0
Damping coefficient of drive and driven sprockets	0.01	0.001	0.001	0
Coulomb friction coefficient for bushing and pin	0	0	0	0.1
Relative error allowed in numerical integration	1×10^{-5}		1×10^{-5}	
Tolerance of separation angle (to check collision)	1×10^{-6} rad		1×10^{-6} rad	
Tolerance of contact force (to check disengagement)	1×10^{-5} N		1×10^{-4} N	

Table 3.1 Reference Values of Parameters Used in the Computer Simulation

Nomenclature

$\mathbf{a}^i$ = acceleration of the mass center of rigid body i

A_{sr} = function of the generalized coordinates and time

$\boldsymbol{\alpha}^i$ = angular acceleration of rigid body i

α^i = the magnitude of the angular acceleration of rigid body i

a_x^i = x component of the acceleration of rigid body i

a_y^i = y component of the acceleration of rigid body i

B_s = function of the generalized coordinates and time

C = point on the sprocket where the roller contacts

C' = point on the roller that comes into contact with the sprocket

d_A = viscous friction coefficient of the rotating axle of the drive sprocket

d_B = viscous friction coefficient of the rotating axle of the driven sprocket

d_L = viscous friction coefficient of the joint between chain links

e = coefficient of restitution

e^i = 1 (i = 0), 1/2 (i = 1, ..., N), or 0 (i = N+1)

F_r = r-th generalized holonomic active force

F_r^* = r-th generalized holonomic inertia force

$\tilde{F}_r$ = r-th nonholonomic generalized active force

$\tilde{F}_r^*$ = r-th nonholonomic generalized inertia force

G = center of the chain link

I^i = central moment of inertia of rigid body i

I_ρ = magnitudes of normal impulse

I_τ = magnitudes of the tangential impulse

k = torsional stiffness of the torsion bars

λ_A = pitch angle of the drive sprocket

λ_B = pitch angle of the driven sprocket

m^i = mass of rigid body i

μ_{PB} = Coulomb friction coefficient of the joint between chain links

μ_{RS} = coefficient of kinetic friction between the roller and the sprocket

N = number of the chain links in the chain span

ν = angle between link 1 and normal vector $\boldsymbol{\rho}$

p^i = radius of the pitch circle of the drive sprocket ($i = 0$), pitch of chain link i ($i = 1, ..., N$), or radius of the pitch circle of the driven sprocket ($i = N+1$)

$q_A(t)$ = angle of rotation of the gear connected to the drive sprocket

$q_B(t)$ = angle of rotation of the gear connected to the driven sprocket

q_r = r-th generalized coordinate

$\boldsymbol{\rho}$ = unit vector normal to the sprocket surface at the contact point and directing inwards

R_P = radius of the pin

R_R = radius of the roller

S = magnitude of the contact force exerted on the disengaging roller by the sprocket or magnitude of vector S

$\mathbf{S}$ = vector denoting the contact force exerted on the disengaging roller by the sprocket

T^i = contributing torque exerted on rigid body i.

$\boldsymbol{\tau}$ = unit vector normal to vector $\boldsymbol{\rho}$ as shown in Fig 2.4

t_1 = initial moment of the collision process

t_2 = final moment of the collision process

T_A = external torque applied to the drive sprocket

T_B = external torque applied to the driven sprocket

$u_k(t_2)$ = k-th generalized speeds at the instant of rebound

u_r = r-th generalized speed

$\dot{u}_k$ = k-th derivative of generalized speed

$\mathbf{v}_{app}$ = velocity of approach of points C and C' at time t_1

$\mathbf{v}^{C'}$ = velocity of point C'

$\mathbf{v}^{C}$ = velocity of point C

$\mathbf{v}^i$ = velocity of the mass center of rigid body i

$\mathbf{v}_{sep}$ = velocity of separation of points C and C' at time t_2

$\tilde{\mathbf{v}}_r^C$ = r-th nonholonomic partial velocity of point C

$\tilde{\mathbf{v}}_r^{C'}$ = r-th nonholonomic partial velocity of point C'

$\boldsymbol{\omega}^i$ = angular velocity of rigid body i

$\boldsymbol{\omega}_r^i$ = r-th holonomic partial angular velocity of rigid body i

ω_r^i = r-th holonomic partial velocity of the mass center of rigid body i

$\mathbf{x}$ = unit vector directing from the center of the drive sprocket to the center of the driven sprocket

X' = $\mathbf{x}$ component of the joint force exerted on the disengaging link by the neighboring link which is fully engaged with the sprocket

X_{i+1} = $\mathbf{x}$ component of the force on the rigid body i by rigid body i+1

ψ = angle defined in Fig. 2.3

$\mathbf{y}$ = unit vector perpendicular to unit vector $\mathbf{x}$ and directing the side of the tight chain span

Y' = $\mathbf{y}$ component of the joint force exerted on the disengaging link by the neighboring link which is fully engaged with the sprocket

Y_{i+1} = $\mathbf{y}$ component of the force on the rigid body i by rigid body i+1

$\mathbf{z}$ = unit vector perpendicular to unit vectors $\mathbf{x}$ and $\mathbf{y}$, or equal to $\mathbf{x} \times \mathbf{y}$

ζ_B = angle defined in Fig. 2.3

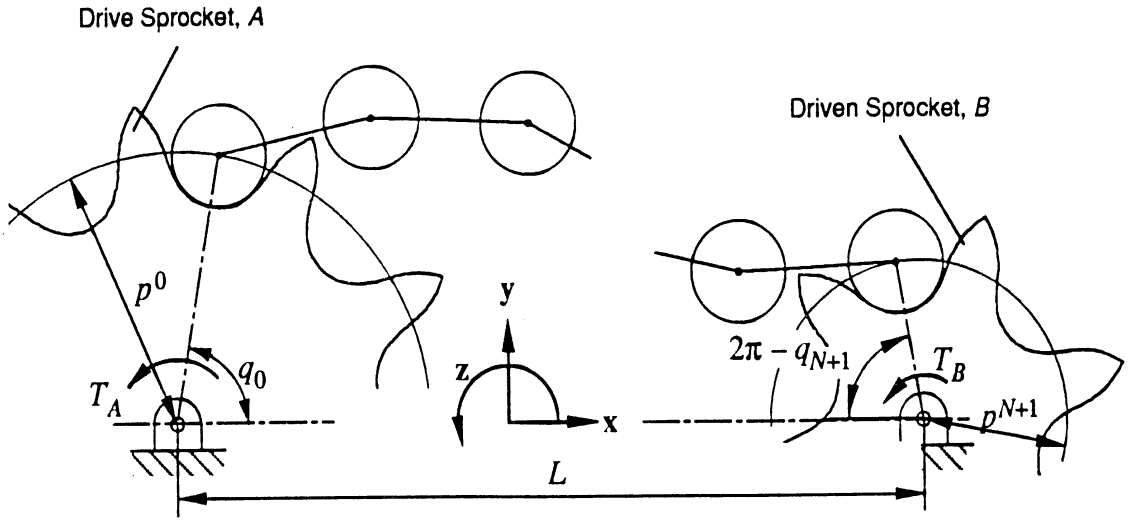

Fig. 2.1 Roller Chain Drive System Model

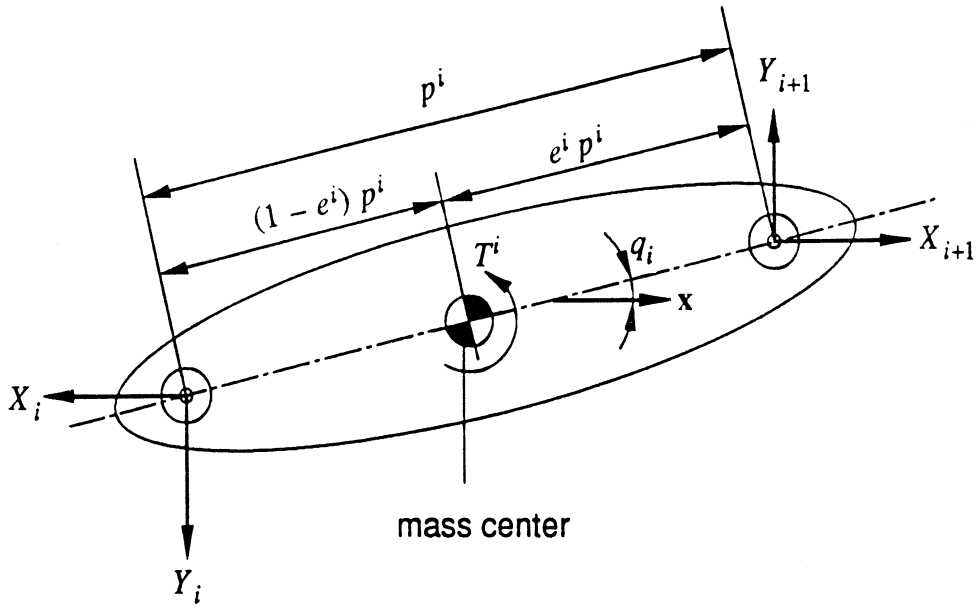

Fig. 2.2 Free-body Diagram of Rigid Body *i*

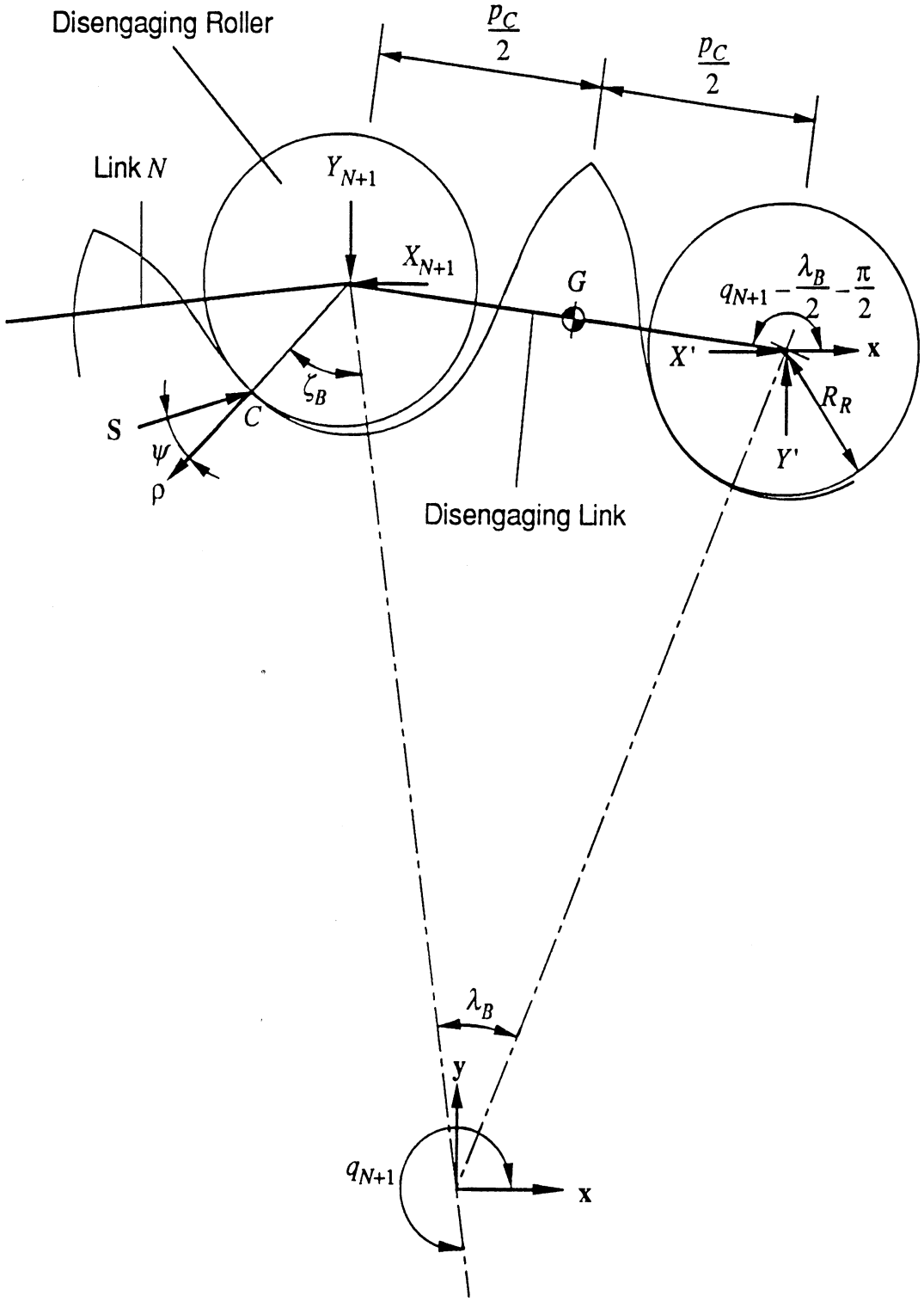

Fig. 2.3 Free-body Diagram of the Disengaging Link

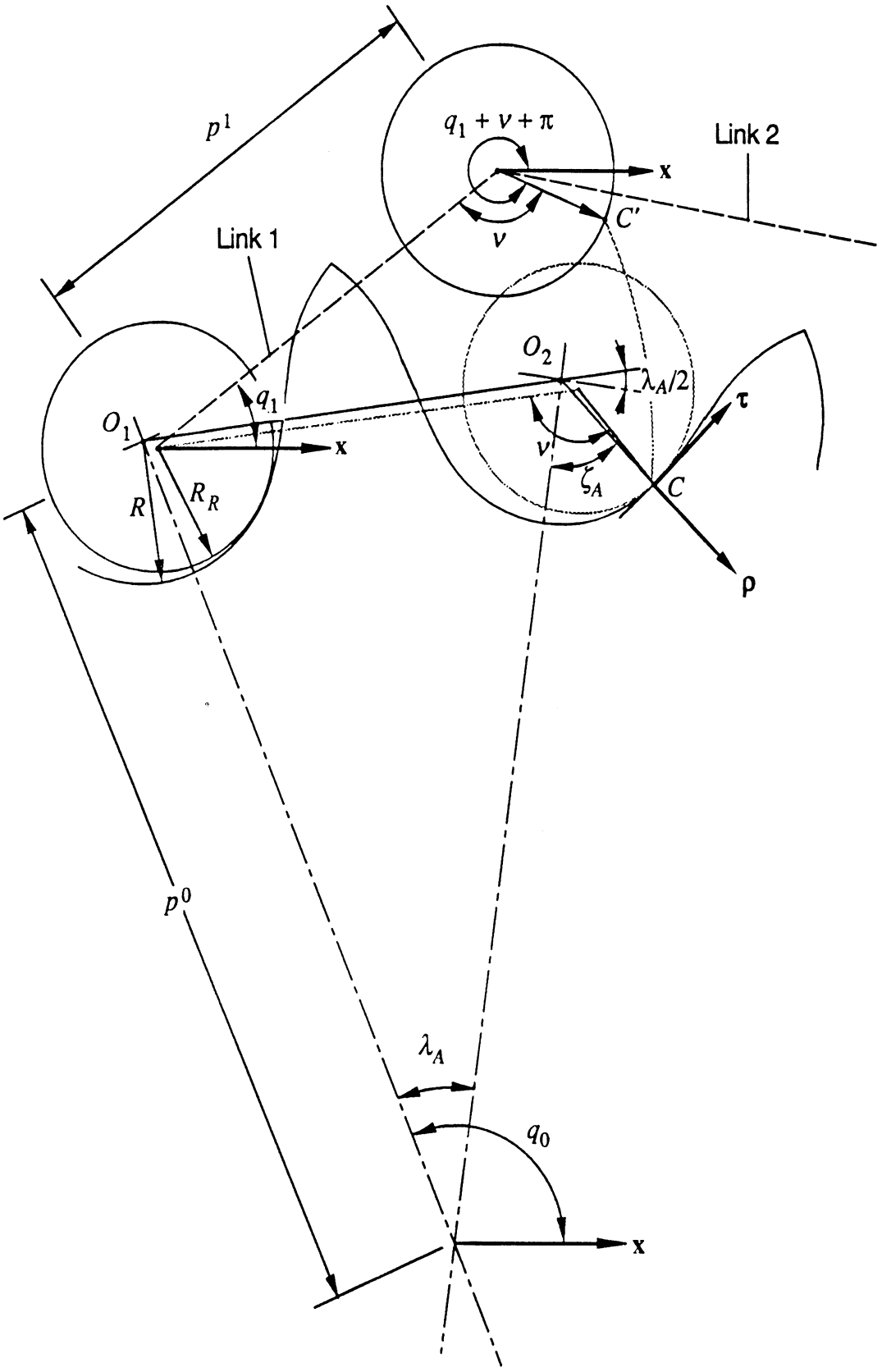

Fig. 2.4 Definition of Angles Relevant to the Engaging Link

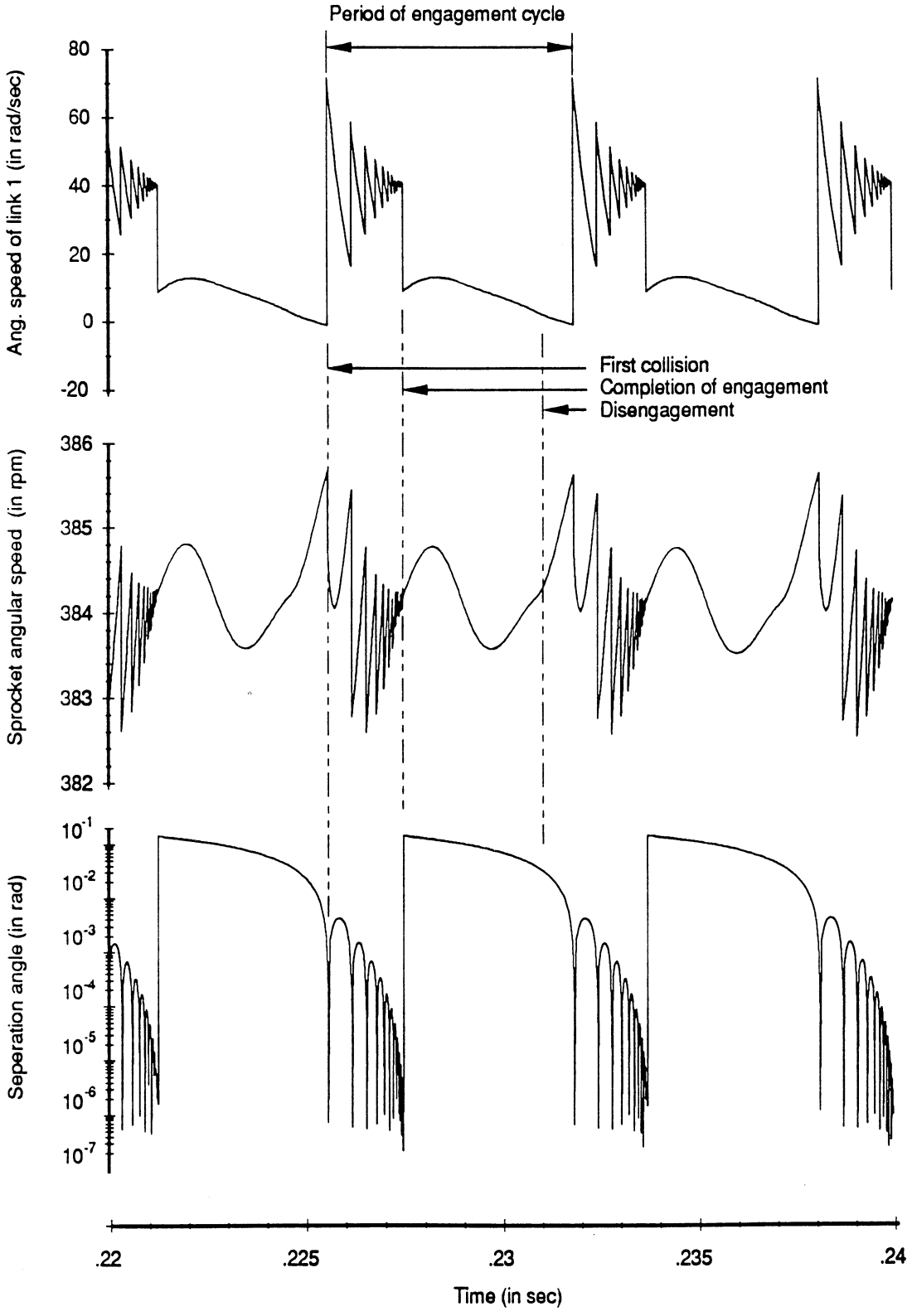

Fig. 4.1 Response of the No. 80 Chain System With Viscous Friction At 384 rpm

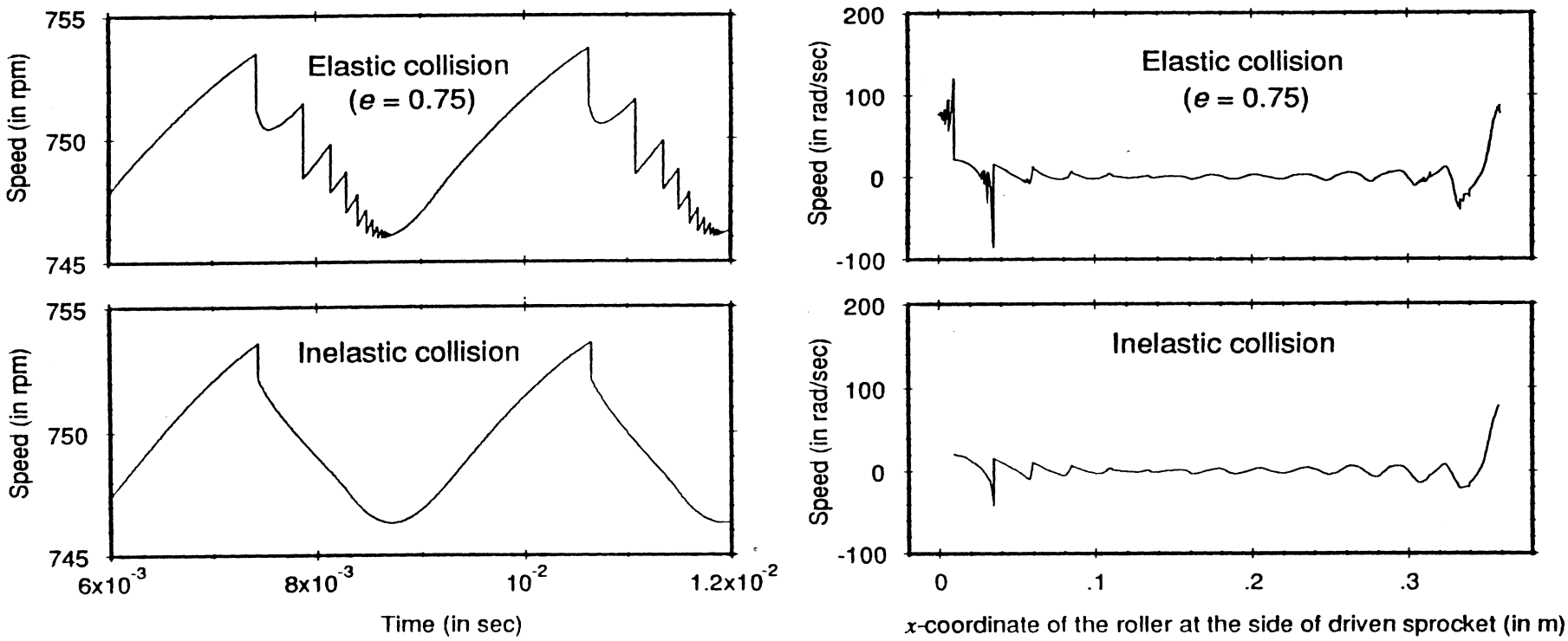

(a) Angular Speed of the Drive Sprocket

(b) Angular Speed of a Chain Link

Fig. 4.2 Angular Velocities of the Drive Sprocket and Chain Links Affected by Modeling of Collision

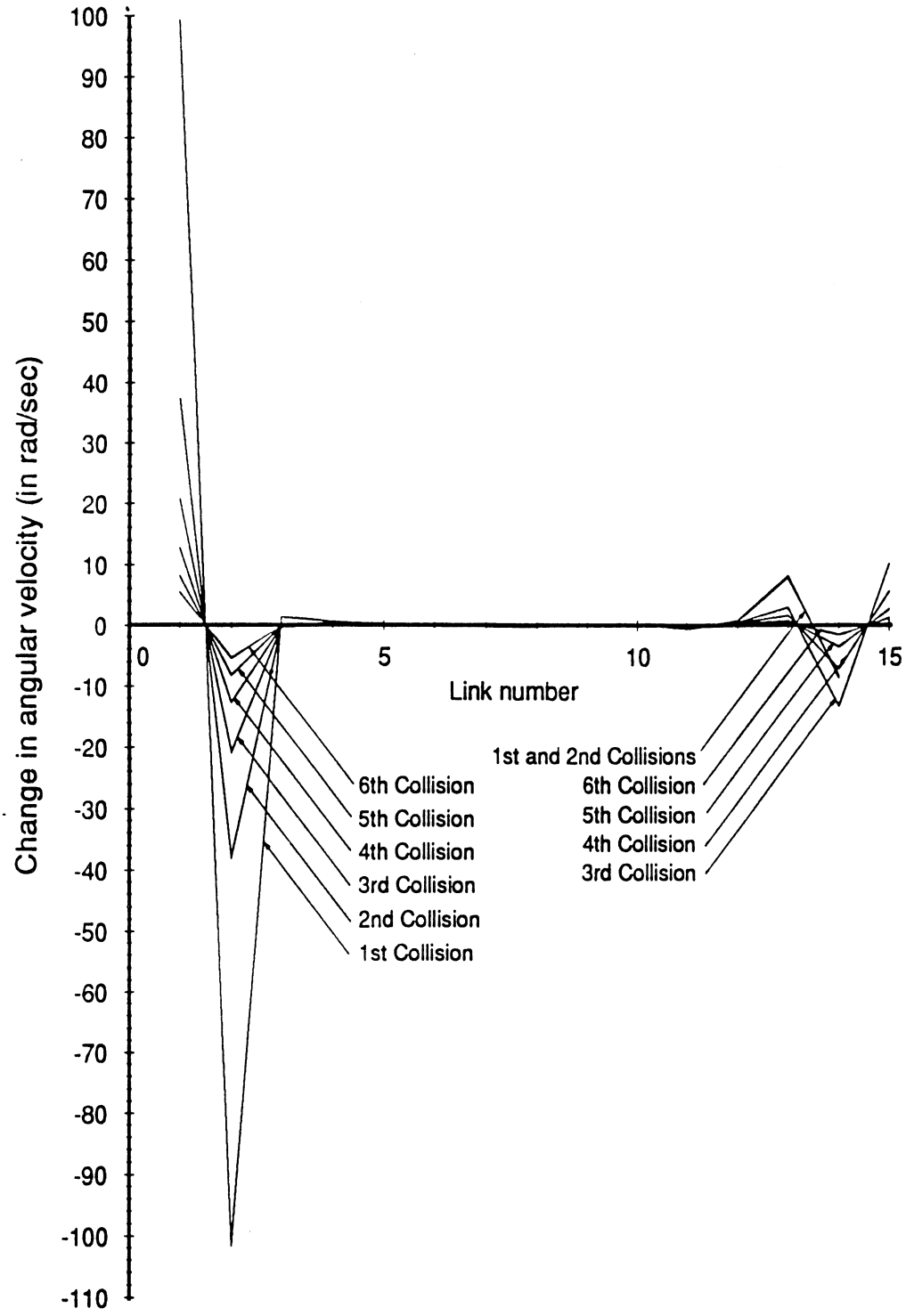

Fig. 4.3 Changes in the Angular Velocities of Chain Links Due to Collision

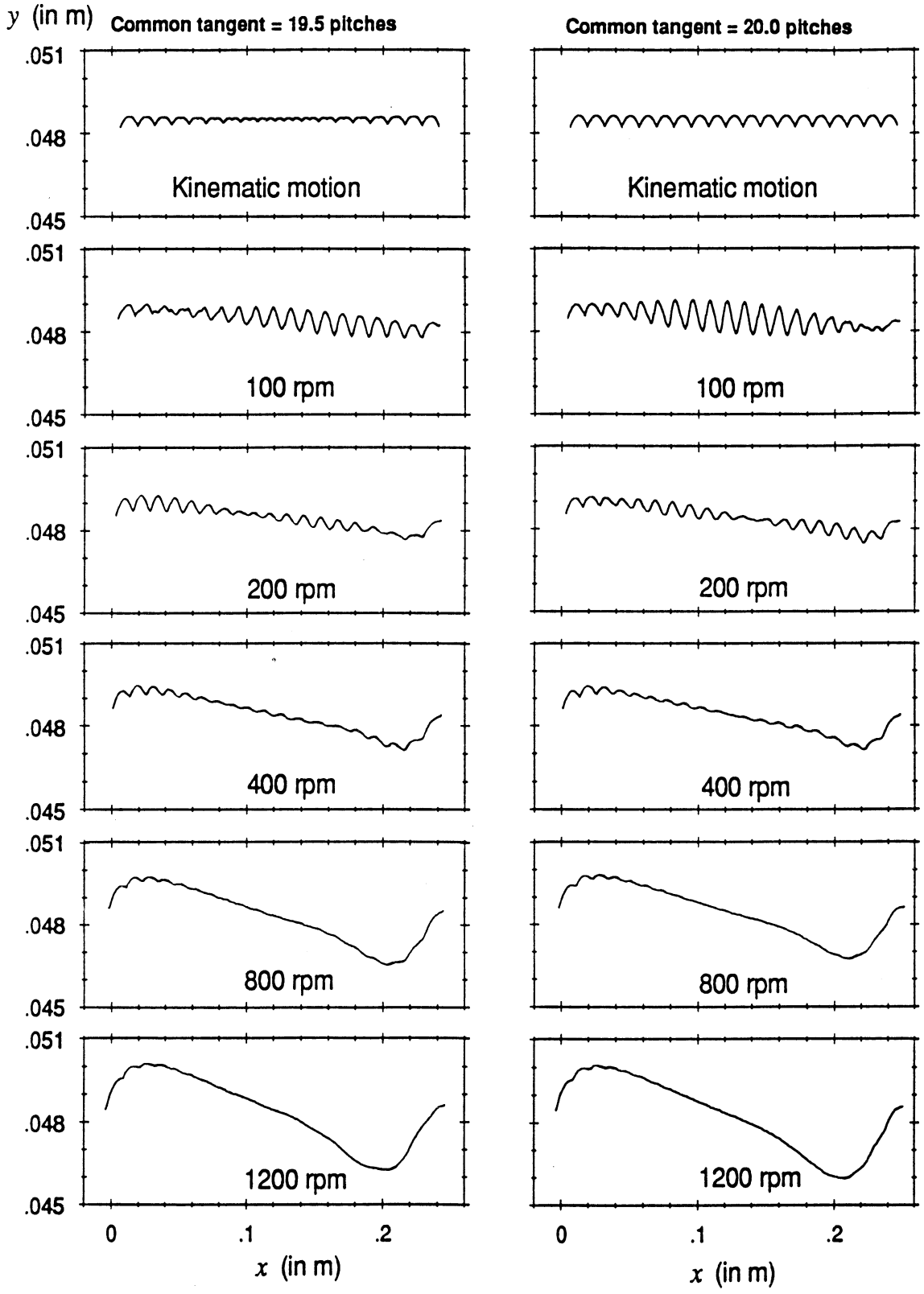

Fig. 4.4 Trajectory of the Center of a Roller of the No. 40 Chain for Common Tangent of 19.5 Pitches (left column) and 20.0 Pitches (right column)

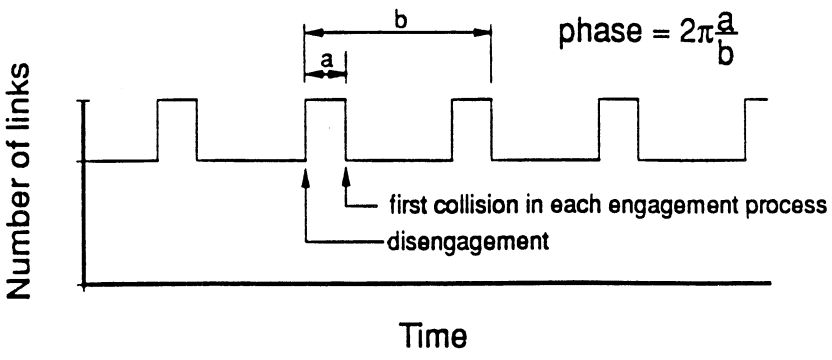

(a) Definition of the Phase between Disengagement and Engagement

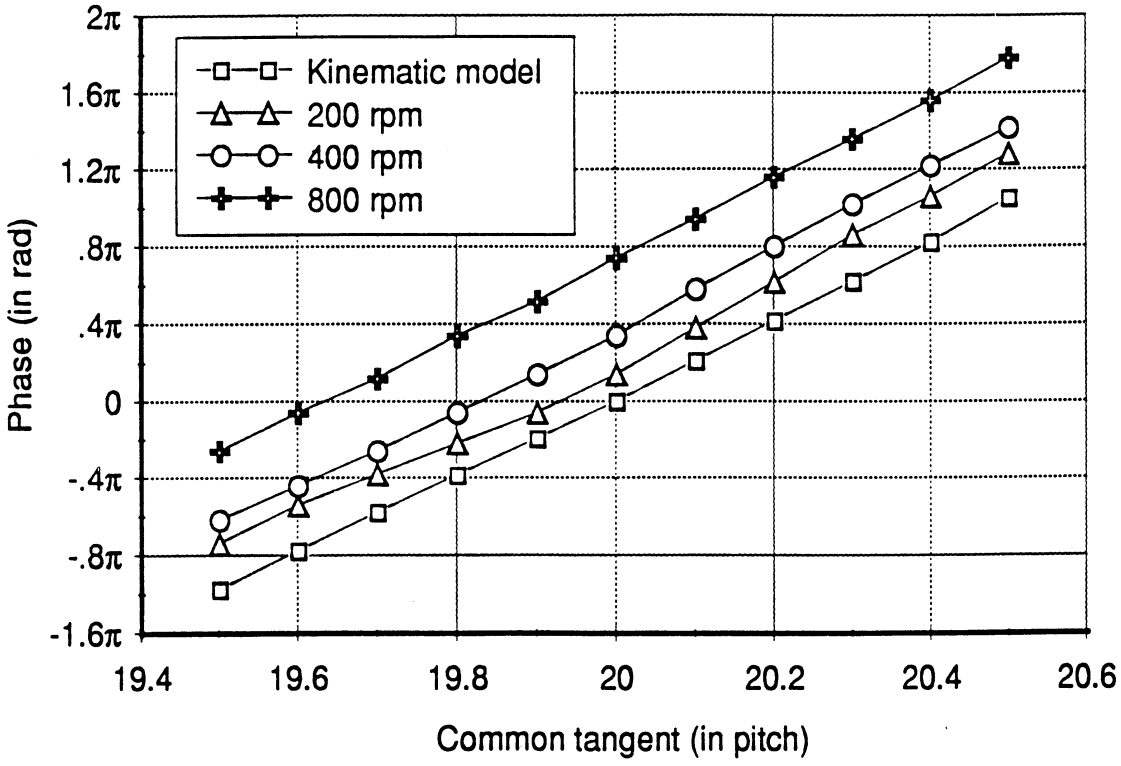

(b) Phase of the No. 40 Chain System with Smaller Friction

Fig. 4.5 Phase between Disengagement and Engagement of the No. 40 Chain System with Smaller Friction

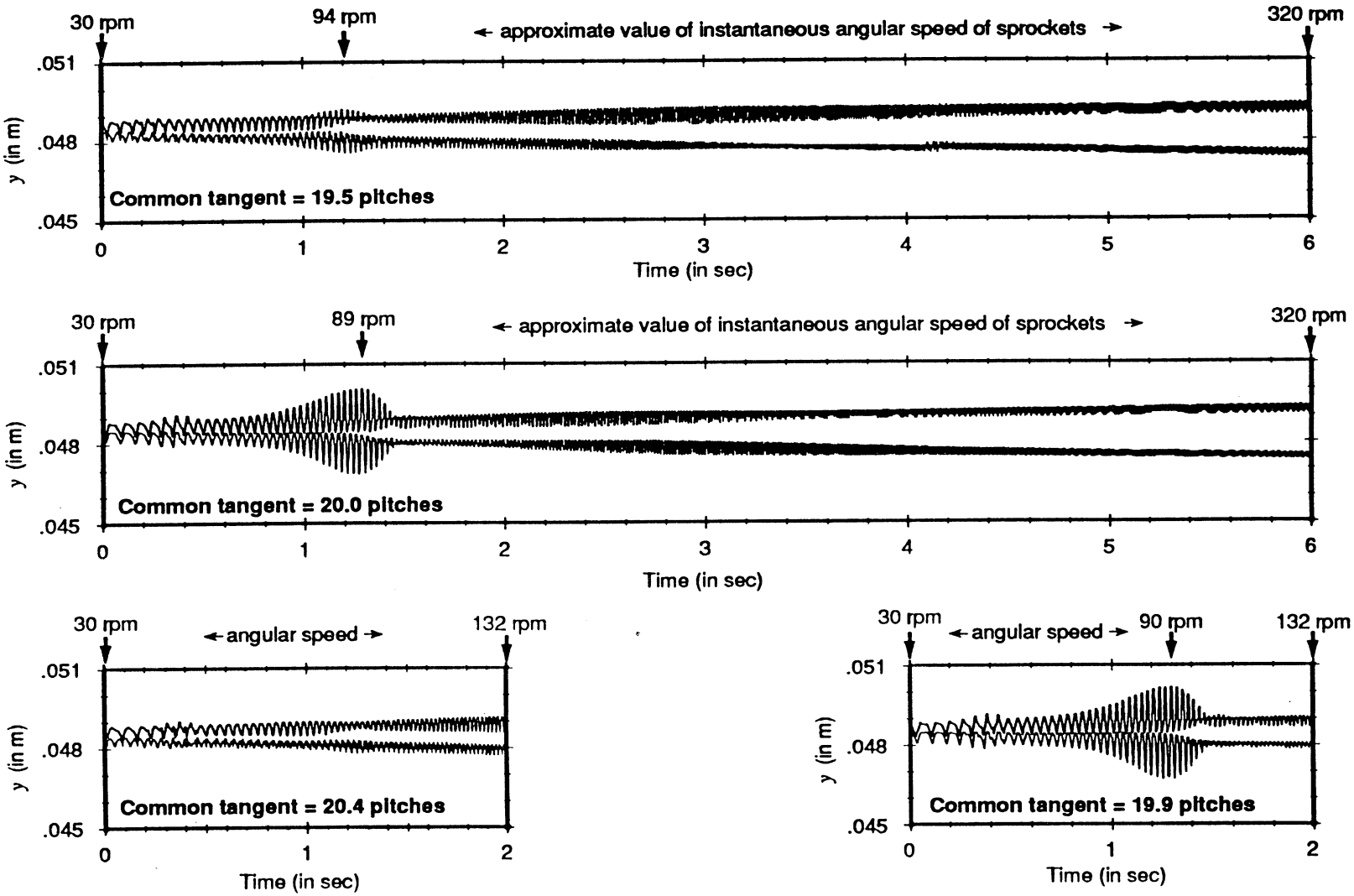

Fig. 4.6 y-coordinate of Extreme Points in the Chain Span of the No. 40 Chain System with Larger Friction

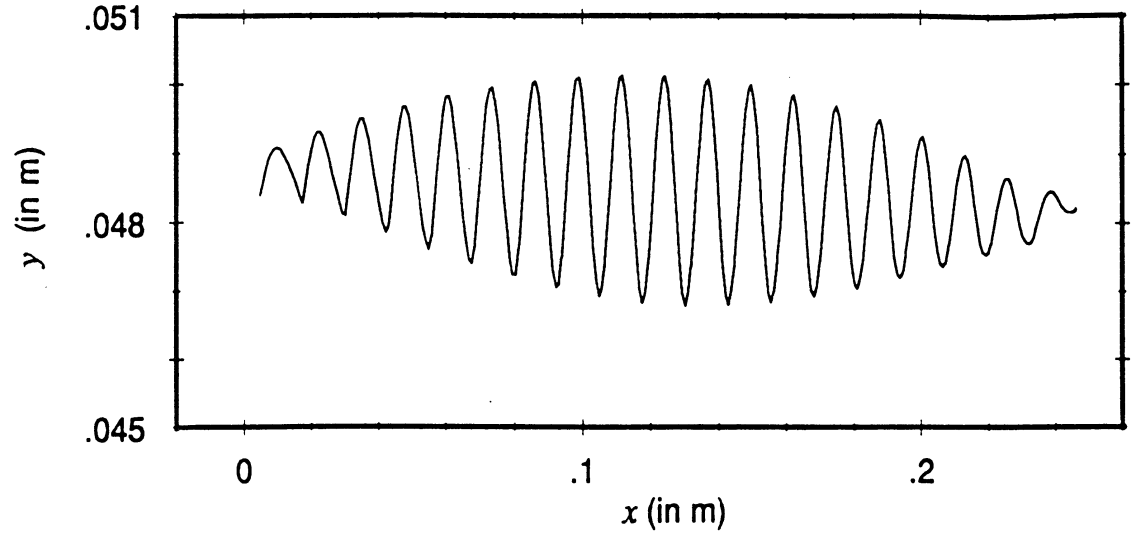

(a) Trajectory of the Center of a Roller

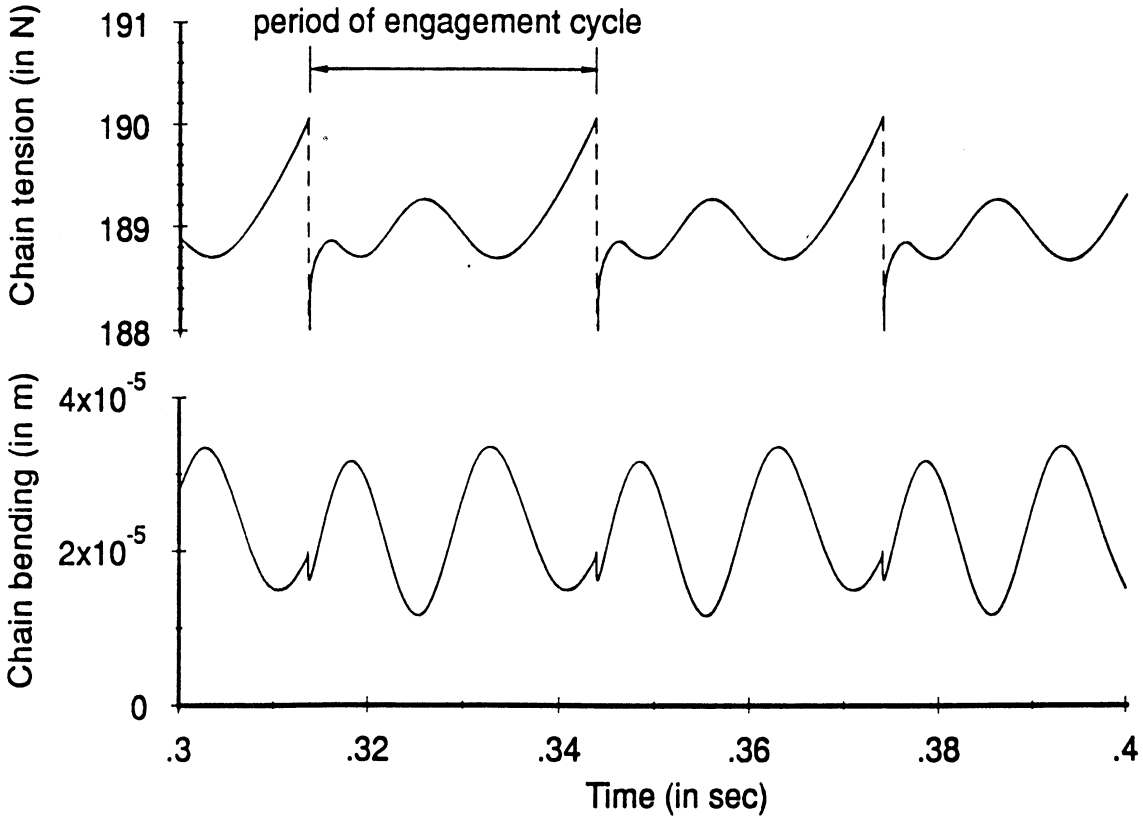

(b) Tension of the Chain Span (top) and the Deviation of the Chain Span from the Straight Line (bottom)

Fig. 4.7 Resonance of the No. 40 Chain System with Larger Friction and Common Tangent of 19.9 Pitches